Version of Record: https://www.sciencedirect.com/science/article/pii/S0029549323001358
Manuscript_02d270612bc995bda2e36cf323421145

Mid-height Seismic Isolation of Equipment in Nuclear Power Plants: Numerical Simulations and Design Recommendations

Kaivalya M. Lal[a*], Andrew S. Whittaker[b], and Mettupalayam V. Sivaselvan[c]

[a] PhD Candidate, Ketter Hall, University at Buffalo, The State University of New York, Amherst, NY 14260
[b] SUNY Distinguished Professor, University at Buffalo, The State University of New York, Amherst, NY 14260
[c] Professor, University at Buffalo, The State University of New York, Amherst, NY 14260
[*] Corresponding author: klal@buffalo.edu

Abstract

Seismic isolation can mitigate earthquake demands on safety-class equipment and is being considered for application to some advanced nuclear reactors. For tall, slender vessels that could represent an advanced reactor, a steam generator or a heat exchanger, mid-height seismic isolation has been shown to be beneficial and practical. This paper focuses on numerical modeling of a mid-height isolated tall, slender vessel with two primary goals 1) investigate and quantify the benefits of mid-height seismic isolation for a range of support structure stiffnesses, isolation systems, and seismic inputs, and 2) provide analysis and design recommendations for isolation of safety-class equipment. Results of response-history analysis were in good agreement with experimental measurements and demonstrated that mid-height isolation can substantially reduce seismic demands on tall, slender vessels for a range of support structure stiffnesses, isolation systems, and seismic inputs. Importantly, the reductions in horizontal spectral accelerations in the mid-height isolated vessel from the non-isolated condition were not affected by the stiffness of the support structure. Recommendations are made for analysis and design of isolated equipment and testing of isolators used for equipment protection in nuclear facilities, which are also applicable to other industries.

Keywords: equipment protection; mid-height seismic isolation; safety-class equipment; nuclear power plants; response-history analyses; design recommendations

1. Introduction

Seismic isolation is an effective means to reduce the effects of earthquake shaking. It can substantially reduce the seismic demands and risk in structures, systems, and components (SSCs) in nuclear power plants (NPPs) (Tajirian (1992), Aiken *et al.* (2002), Huang *et al.* (2008; 2009), Kumar *et al.* (2017a; 2017b), Yu *et al.* (2018)), but is yet to be applied to an NPP (or a nuclear facility) in the United States. Seismic base isolation is being considered as an integral design feature in a number of US advanced nuclear reactors to enable deployment of standardized plants with significantly lower costs (Lal *et al.*, 2022; Parsi *et al.*, 2022). An alternate implementation, where base isolation of reactor buildings is impractical, would involve isolation of individual pieces of safety-class equipment at their supports inside a nuclear facility.

Design and licensing of advanced nuclear reactors will rely on seismic analysis tools that can predict the response of isolated equipment and its isolation system for multidirectional earthquake inputs. There are only a few earthquake-simulator studies of isolated equipment presented with companion numerical predictions of response. Ersoy *et al.* (2001), Murota *et al.* (2005), and Oikonomou *et al.* (2016) tested models of power transformers isolated using rubber and spherical sliding bearings. The predictions of the measured responses of the isolated transformer were good. Kong (2010) performed earthquake-simulator experiments on a 230 kV disconnect switch isolated using wire rope isolators and Friction Pendulum bearings and predicted responses with acceptable accuracy. Lee and Constantinou (2017; 2018) tested a transformer model similar to that of Oikonomou *et al.* (2016) equipped with a passive three-dimensional (3D) seismic isolation system that consisted of spherical sliding bearings providing horizontal isolation, supported atop guided spring-damper devices for vertical isolation. The predicted responses were in good agreement with the test data. Mir *et al.* (2022a) conducted earthquake-simulator experiments on a base-isolated model of a fluoride-salt cooled high temperature reactor that involved representations of a prototype reactor vessel, a core barrel, reflector blocks in the vessel, a coolant fluid, and spherical fuel pebbles. Responses of the vessel, its components, and the isolation system were recovered with good accuracy using the finite element models.

All these past studies have focused on base isolating equipment, which may not be practical for tall, slender vessels due to the large base overturning moments that can develop during extreme earthquake shaking, resulting in substantial tensile axial forces or possible uplift in the bearings. Lal *et al.*, (2023a; 2023b) proposed a novel strategy involving mid-height seismic isolation of tall, slender vessels and conducted earthquake-simulator experiments to demonstrate that it is beneficial and practical. Herein, numerical models are developed for the test specimen of Lal *et al.*, (2023a; 2023b). The goals of modeling are to 1) investigate the utility and quantify the benefits of mid-height seismic isolation, and 2) provide analysis and design recommendations for seismic isolation of safety-class equipment. Prior to performing response-history analyses supporting the two goals, numerical models were benchmarked by comparing predicted responses with the test data of Lal *et al.*, (2023a; 2023b).

The test specimen of Lal *et al.*, (2023a; 2023b) was a half-length scale, 240-inches tall, cylindrical, carbon steel vessel with an outer diameter of 60 inches and a wall thickness of 1 inch. It was supported at its mid-height, near its center of gravity, on a stiff steel frame using three equally spaced radial mounts. The mounts were welded to the vessel wall and connected to each other via shaped plates to achieve diaphragm action above the isolation plane. The steel frame had plan dimensions of 116 in $\times$ 116 in and was 121 inches tall. The frame had four corner columns concentrically braced with angles to provide lateral stiffness, and three interior columns, one beneath each support mount, to provide vertical support to the vessel. The corner columns were joined by 6-inch deep by 1-inch thick plates, welded to a 1-inch thick mounting plate with a central 76-inch diameter hole. The 1-inch thick plate atop the support frame provides diaphragm action below the isolation plane. Figure 1 shows the test assembly installed on the earthquake simulator. Three configurations of the vessel were tested: 1) non-isolated, 2) isolated using single Friction Pendulum (SFP) bearings with a sliding period of 1.38 seconds, and 3) isolated using triple Friction Pendulum (TFP) bearings with a sliding period of 1.95 seconds. The vessel was filled with water during testing to indirectly account for the fluid and internal equipment inside a prototype vessel. The total weight of the vessel, including water, was approximately 40 kips, and that of the support frame was 10 kips.

The vessel was subjected to three component ground motions (GMs) using a 6 degrees-of-freedom earthquake simulator at the University at Buffalo. Three ground motions were selected from the PEER NGA-West 2 database to cover a broad range of frequencies: from approximately 0.2 Hz to 45 Hz in the two horizontal directions (H1 and H2) and 0.2 Hz to 70 Hz in the vertical direction (V). The frequency range of interest was determined based on modal analyses of a preliminary numerical model of the test specimen. The selected ground motions were: 1) Record Sequence Number (RSN) 587, peak ground acceleration (PGA) H1 = 0.28 g, H2 = 0.24 g, V = 0.14 g, 2) RSN 728, PGA H1 = 0.17 g, H2 = 0.21 g, V = 0.23 g, and 3) RSN 796, PGA H1 = 0.10 g, H2 = 0.20 g, V = 0.06 g. The time scale of all three components of the ground motions was compressed by a factor of 0.71, consistent with the assumed length scale of 0.5. Figure 2 presents 5% damped acceleration response spectra of the time-scaled ground motions. The ground motions were amplitude scaled to achieve different intensities of shaking. Earthquake-simulator tests were performed using unidirectional (1D), bi-directional (2D), and tri-directional (3D) inputs. This paper focuses on the 3D tests and 3D simulations, to achieve the two goals identified above. The 3D test sequences for the non-isolated, SFP-isolated, and TFP-isolated configurations are presented in Table 1. Experiment data for all the tests (1D, 2D, and 3D tests) are archived at DesignSafe.

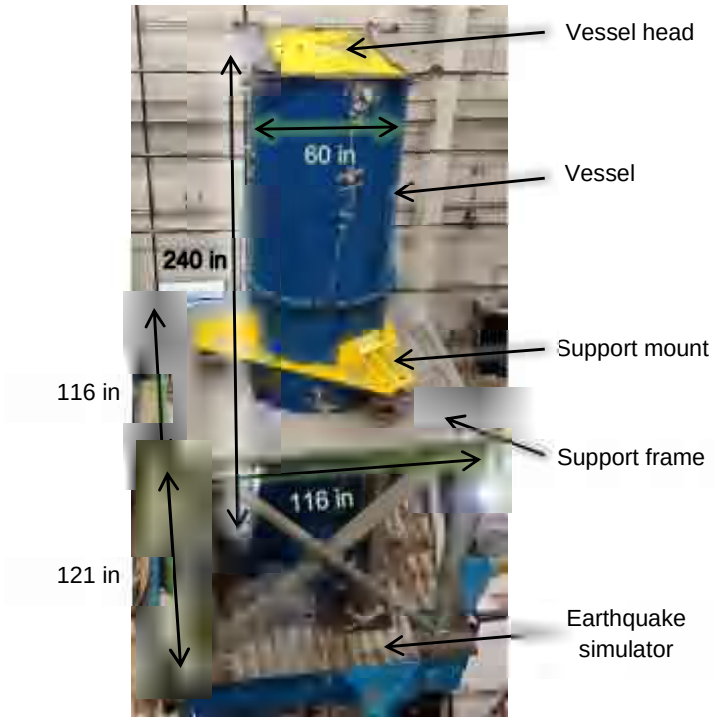

Figure 1. Test assembly on the earthquake simulator

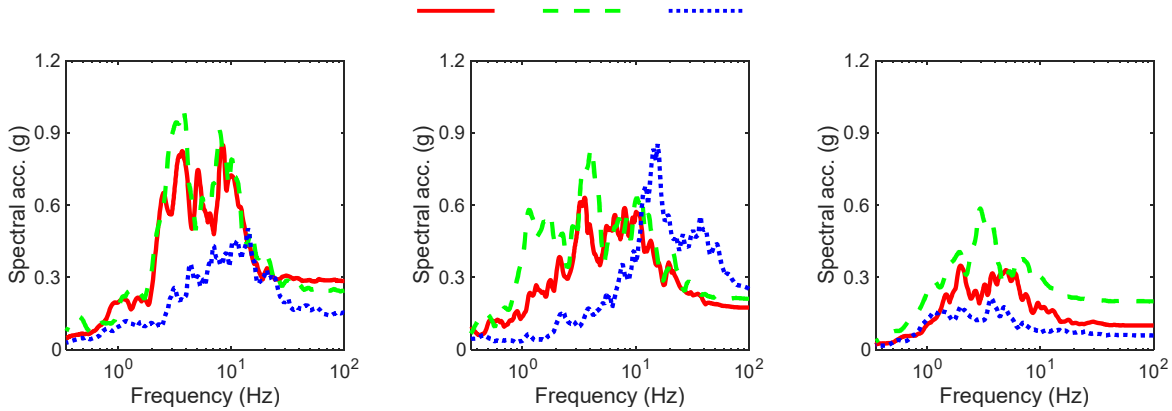

a) GM1 b) GM2 c) GM3

Figure 2. Acceleration response spectra of the time-scaled ground motions, 5% damping

Table 1. 3D test sequence

#	Test	Geomean horizontal PGA (g)[1]	Vertical PGA (g)
	Non-isolated vessel		
1	FB1A-3D	0.20	0.11
2	FB1B-3D	0.40	0.22
3	FB2A-3D	0.20	0.25
4	FB2B-3D	0.35	0.43
5	FB3A-3D	0.10	0.04
6	FB3B-3D	0.25	0.10
	SFP-isolated vessel		
1	SF1A-3D	0.20	0.11
2	SF1B-3D	0.60	0.33
3	SF2A-3D	0.20	0.25
4	SF2B-3D	0.35	0.43
5	SF3A-3D	0.10	0.04
6	SF3B-3D	0.25	0.10
	TFP-isolated vessel		
1	TF1A-3D	0.20	0.11
2	TF1B-3D	0.60	0.33
3	TF2A-3D	0.20	0.25
4	TF2B-3D	0.50	0.61
5	TF3A-3D	0.10	0.04
6	TF3B-3D	0.30	0.12

1. $\sqrt{\text{PGA of H1} \times \text{PGA of H2}}$

2. Numerical modeling and benchmarking

2.1. Introduction

Three numerical models were developed in the computer program SAP2000 (CSI, 2021), one each for the non-isolated, SFP-isolated, and TFP-isolated configuration. Figure 3a presents an isometric view of the non-isolated numerical model. The vessel (red in Figure 3a), its flanges (blue), support mounts and the shaped plates (yellow), vessel head (green), and the mounting plate of the support frame (grey) were modeled using shell elements with thicknesses matching the test specimen of Lal *et al.*, (2023a; 2023b). The columns and angles of the support frame were modeled using beam elements with section properties per those used for the fabrication of the test specimen.

Mechanical properties consistent with carbon steel were assigned to the shell and the beam elements. The bottom nodes of the columns and angles, where the support frame was bolted to the earthquake-simulator platform, were assigned a ***fixed*** joint restraint in all six degrees-of-freedom. The SAP2000 model was calibrated to the measured rocking frequencies of the non-isolated configuration by reducing a) the stiffness of the support frame members by 15% (to account for the flexibility of the connections between the members of the support frame), and b) membrane, bending, and shear stiffnesses of the support mounts and the shaped plates by 15% (to account for the flexibility of the welded connections).

The fluid response was treated as impulsive[1], and interaction of the fluid and the surrounding structure (vessel) was ignored: an appropriate assumption as the vessel was filled with water, leaving no room for sloshing. The weight of the water (= 23 kips) was distributed uniformly along the height of the vessel wall (red in Figure 3a) using area mass for shell elements in SAP2000[2].

Five-channel load cells (placed beneath the bearings in earthquake-simulator experiments to measure reaction forces) and the Friction Pendulum (FP) bearings were modeled using two joint links. The ***Linear Spring*** element was assigned to the load cell links, with horizontal and vertical stiffnesses per Appendix A of Mir ***et al.*** (2022b). The rotational degrees of freedom for the load cell links were ***fixed*** as the they have high rotational stiffness. The bottom node of the load cell links was connected to the mounting plate of the support frame, directly above the beam elements for the interior columns of the support frame, and the top node to the underside of the support mounts of the vessel: see Figure 3b. The ***Friction Isolator*** and ***Triple Pendulum Isolator*** elements were assigned to the bearing links for modeling SFP and TFP isolators, respectively, with the radius of curvature, coefficients of friction, rate parameter, and axial stiffness per the bearing test data of Lal ***et al.*** (2023b). The isolator links were modeled atop the load cells links: see Figure 3c.

2.2. Modal analysis

Modal analysis was performed to compare predicted and measured resonant frequencies. Table 2 presents results. Translational modal frequencies in the ***x*** and ***y*** directions could not be clearly identified from the experimental data because rocking of the vessel dominated its translational response (Lal ***et al.***, (2023a; 2023b)). In the ***z*** direction, the SAP2000 model overestimated the first translational frequency in all three configurations: the sources of the difference could not be clearly identified but are attributed to connections, including those associated with the support mounts. The close agreement between the predicted and measured rocking frequencies is an outcome of the calibration exercise described previously in Section 2.1. For the isolated configurations, the axial flexibility of the bearings needed to be accurately modeled to recover the rocking frequencies. (Lal ***et al.*** (2023b) characterized the axial flexibility by individual testing of bearings.)

---

[1] Studies on fluid-structure-interaction parse hydrodynamic response of a fluid in a dynamically excited vessel into impulsive and convective components. The impulsive response is from the part of the fluid that moves (and accelerates) with the vessel. The convective response is from the part of the fluid that oscillates and forms waves on the free surface (sloshing).

[2] At the time of this writing, SAP2000 does not have the ability to explicitly model fluid-structure-interaction, for which other finite element programs (e.g., LS-DYNA and ABAQUS) can be used (see Yu and Whittaker (2020) and Mir ***et al.***, (2022b))

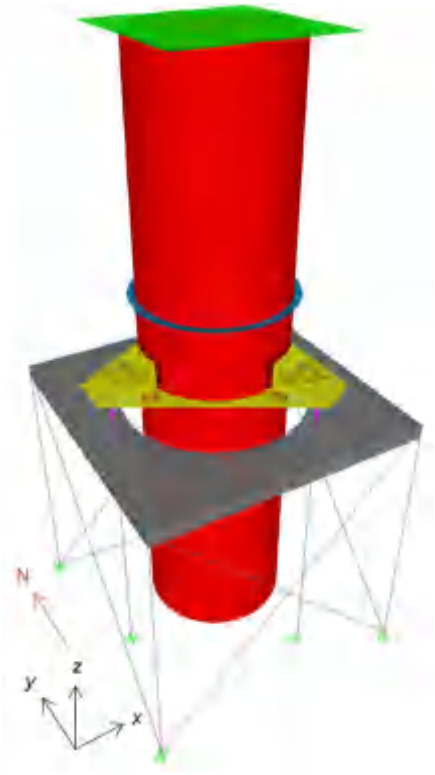

a) isometric view

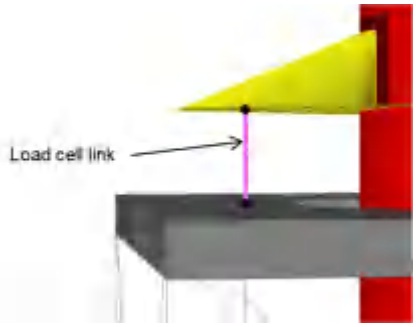

b) close-up view of the load cell link in the non-isolated configuration

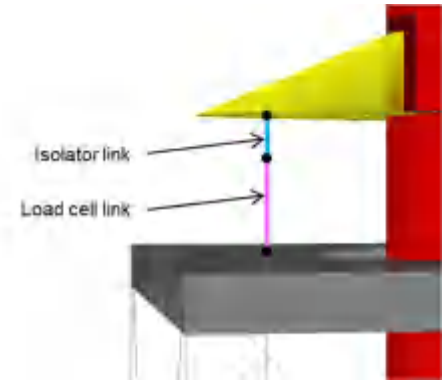

c) close-up view of the load cell and isolator links in the isolated configurations

Figure 3. Numerical model of the test specimen in SAP2000

Table 2. Resonant frequencies from the SAP2000 model and test data[1]

	x and *y* directions[2]		R_x and R_y directions[2]		*z* direction[2]	
	SAP2000	Test data	SAP2000	Test data	SAP2000	Test data
Non-isolated	14 Hz[3]	NA[4]	10.4 Hz	11 Hz	27 Hz	17 Hz
SFP-isolated	0.72 Hz[5]	NA[6]	8.4 Hz[7]	8 Hz[7]	20 Hz[7]	15.3 Hz[7]
TFP-isolated	0.53 Hz[8]	NA[6]	8.3 Hz[7]	8 Hz[7]	19.6 Hz[7]	15.5 Hz[7]

1. Measured frequencies for the non-isolated vessel were derived by Lal *et al.*, (2023a; 2023b) from low-amplitude system identification tests using multisine excitation. Frequencies for the isolated vessels were derived by analysis of data from the seismic tests.
2. See Figure 3 for the global coordinate system.
3. Corresponds to the horizontal modes of the support frame.
4. Could not be clearly identified as the behavior of the test specimen was driven by the rocking of the vessel.
5. Corresponds to the sliding period of the SFP bearings of 1.38 seconds.
6. Could not be identified from the test data.
7. Lower than in the non-isolated configuration because of the added flexibility of the bearings.
8. Corresponds to the sliding period of the TFP bearings of 1.95 seconds.

2.3. Response-history analyses and damping specifications

Response-history analyses were performed using the Fast Nonlinear Analysis method in SAP2000, with the only nonlinear elements being the isolator links. The acceleration histories recorded at the center of the earthquake-simulator platform during the experiments were used as inputs to the numerical models. Rocking acceleration histories of the platform about the *x*- and *y*-axes were determined by calculating the difference in vertical (*z*) acceleration responses and dividing by the distance between the accelerometers. There were no rocking inputs to the earthquake simulator but rocking of the platform resulted from simulator-specimen interaction and compliance in the simulator's horizontal and vertical actuators (Lal *et al*., 2023b). Prior to the start of a response-history analysis of the isolated configurations, a vertical acceleration of 1 g was imposed to develop gravity load on the isolators, applied gradually over a period of 10 seconds, and followed by an idle time of 5 seconds for the load to stabilize.

Damping in the SAP2000 model was specified using the *Constant Damping with Override* option. This option enables the analyst to select a baseline damping ratio (e.g., 1.5% of critical) for all modes bar some for which an alternate value is specified (i.e., the override). Herein, a constant damping ratio of 1.5% was specified as the baseline value based on analysis of data from tests of the non-isolated configuration. Exceptions to the baseline value were derived from the system identification test results in Lal *et al*. (2023b) and analysis of data from seismic tests: 1) in the non-isolated configuration, an override of 2.5% (4.6%) was applied to the rocking of the vessel about the *x* (*y*) axis; 2) in the isolated configurations, a) an override of 0% was specified for the isolated modes because the energy dissipation in those modes is hysteretic (see Sarlis and Constantinou (2010)), and b) an override of 4.6% was applied to the rocking of the vessel about both *x* and *y* axes. Damping for rocking about the *x* and *y* axis was associated with the oil columns in the simulator's actuators and varied with the frequency content and intensity of the seismic input. A calibration exercise was not performed to determine damping ratios for each seismic input and intensity. Rather a single set of values were used to predict responses for all tests such that the rocking responses were recovered reasonably well by the SAP2000 models across a wide range of intensities.

2.4. Comparison of numerical and experimental results

2.4.1. Overview

The numerical models were benchmarked by comparing predicted results with experiment data. The solid pink circles in Figure 4 identify locations on the test specimen where results from numerical models were extracted, which include:

1. Acceleration time series in *x*, *y*, and *z* directions (global coordinate system is defined in Figures 3 and 4):
    a. Atop the load cells on the north-east side (location ***F1*** in Figure 4), representing acceleration response at the mid-height of the vessel for the non-isolated configuration and directly below the isolation plane for the isolated configurations. (North is defined in Figures 3a and 4.)
    b. On the north-east support mount of the vessel (location ***V1***), representing acceleration response directly above the isolation plane for the isolated configurations.
    c. At the top and the bottom of the vessel on the north face (locations ***V2*** and ***V3***).
2. Isolation-system displacement and force histories, presented as normalized force-displacement loops, derived by normalizing the total horizontal force in the three isolator links by the total instantaneous normal load at the same time step. Identical displacement histories were obtained for the three isolator links, and the *x*- and *y*-direction histories for the north-east link were utilized for generating the force-displacement loops.

Rocking accelerations about the *x*- and *y*-axis at the top and the bottom of the vessel were derived by calculating the difference in the vertical (*z*) acceleration responses and dividing by the horizontal distance between the output stations in SAP2000. Sections 2.4.2, 2.4.3, and 2.4.4 next present the predicted (SAP2000) and measured (test) responses. Section 2.4.5 discusses on the predicted and measured results.

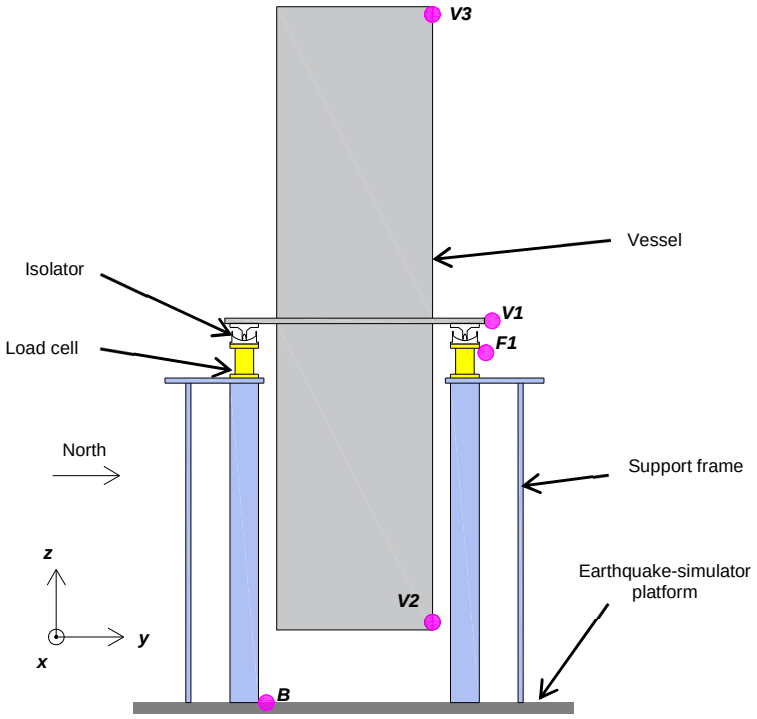

Figure 4. Locations for extracting results from response-history analyses

2.4.2. Non-isolated configuration

Figures 5 and 6 enable a comparison of predicted and measured acceleration spectra at the top and the bottom of the non-isolated vessel for one of the six 3D tests: FB1B-3D. Other comparisons are presented in Lal *et al.* (2023b). Table 3 presents the peak accelerations, derived as spectral acceleration at 100 Hz[3], at the top, bottom, and mid-height of the vessel, and the absolute percentage difference between the numerical and experimental values for the six 3D tests. Peak acceleration is used here as a measure of seismic input to safety-related equipment at the head and the base of the vessel.

The acceleration responses predicted by the numerical model in the two horizontal directions and for rocking about the *x*- and *y*-axis are in good agreement with the test data, with an average difference of 13% (range: 0% to 35%) in the peak horizontal accelerations. Greater differences are seen in the peak vertical accelerations, equal to 24% on average (range: 0% to 48%), due in large part to the significant differences between the measured and predicted frequencies in the *z* direction (see Section 2.2).

2.4.3. SFP-isolated configuration

Figures 7 through 10 enable a comparison of numerical and experimental results for the SFP-isolated vessel for one of the six 3D motions: SF1B-3D. Other comparisons are presented in Lal *et al.* (2023b). Because the acceleration response of the isolated vessel in the two horizontal directions was substantially smaller than in the vertical direction, the *y*-axis range for the *x*- and *y*-direction spectra is different than in the *z* direction. In Figure 7, the peaks at 20 Hz in the predicted horizontal spectra above the isolation plane correspond to the vertical mode of the isolated vessel (i.e., isolators, support mounts, and vessel; see column 6, z direction, SAP2000, in Table 2), which is coupled with the horizontal response. These peaks at 20 Hz were not present in the experimental data because the measured frequency of the isolated vessel was 15 Hz.

[3] Acceleration time series from SAP2000 were processed with a low-pass filter at 100 Hz and so peak accelerations were taken as spectral acceleration at 100 Hz.

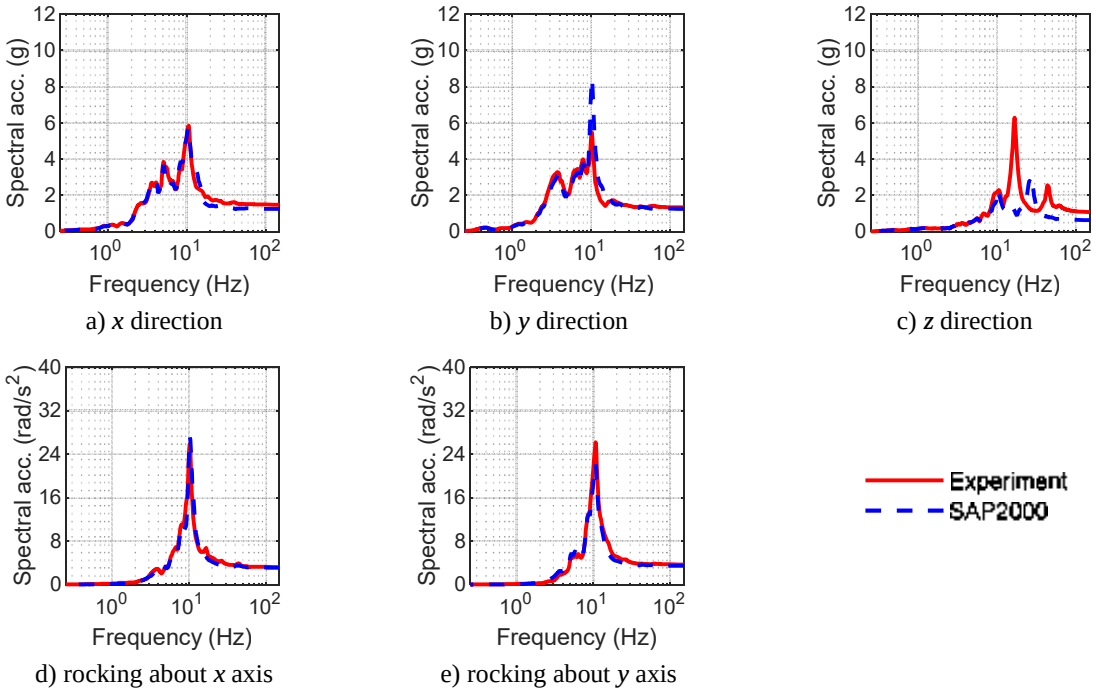

Figure 5. Acceleration response spectra at the top of the vessel, test FB1B-3D

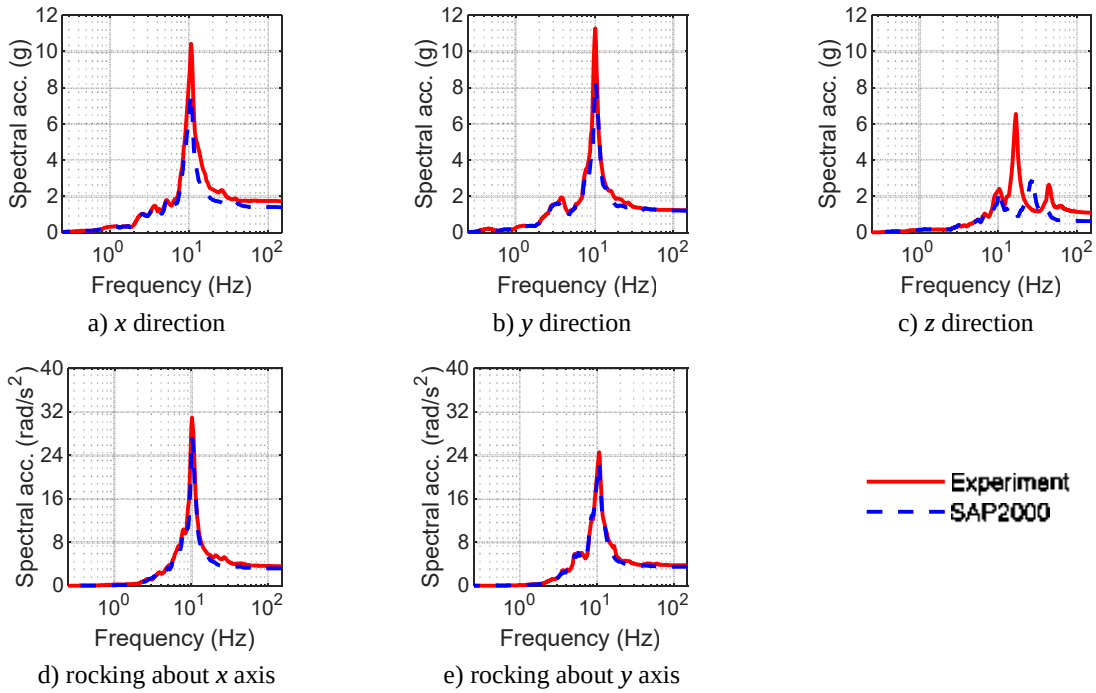

Figure 6. Acceleration response spectra at the bottom of the vessel, test FB1B-3D

Table 3. Peak accelerations[1] (g) for the 3D tests in the non-isolated configuration

Test		Mid-height of vessel			Vessel bottom			Vessel top		
		x	***y***	***z***	***x***	***y***	***z***	***x***	***y***	***z***
FB1A-3D	Experiment	0.34	0.33	0.32	0.72	0.65	0.46	0.67	0.66	0.44
	SAP2000	0.34	0.30	0.20	0.66	0.60	0.36	0.58	0.62	0.35
	Diff (%)	0	9	38	8	8	22	13	6	20
FB1B-3D	Experiment	0.68	0.69	0.73	1.73	1.24	1.07	1.47	1.32	1.04
	SAP2000	0.64	0.63	0.38	1.40	1.21	0.62	1.24	1.25	0.62
	Diff (%)	6	9	48	19	2	42	16	5	40
FB2A-3D	Experiment	0.39	0.35	0.57	0.96	0.47	0.86	0.55	0.50	0.83
	SAP2000	0.35	0.40	0.35	0.62	0.56	0.72	0.59	0.52	0.70
	Diff (%)	10	14	39	35	19	16	7	4	16
FB2B-3D	Experiment	0.72	0.63	0.98	1.69	0.85	1.44	0.98	0.93	1.39
	SAP2000	0.61	0.79	0.62	1.29	0.99	1.29	1.08	0.96	1.28
	Diff (%)	15	25	37	24	16	10	10	3	8
FB3A-3D	Experiment	0.16	0.20	0.06	0.16	0.26	0.08	0.22	0.34	0.08
	SAP2000	0.13	0.20	0.06	0.11	0.21	0.10	0.18	0.30	0.10
	Diff (%)	19	0	0	31	19	25	18	12	25
FB3B-3D	Experiment	0.38	0.51	0.18	0.45	0.63	0.23	0.56	0.85	0.22
	SAP2000	0.34	0.54	0.14	0.31	0.54	0.20	0.47	0.79	0.20
	Diff (%)	11	6	22	31	14	13	16	7	9

1. Peak acceleration taken as spectral acceleration at 100 Hz.

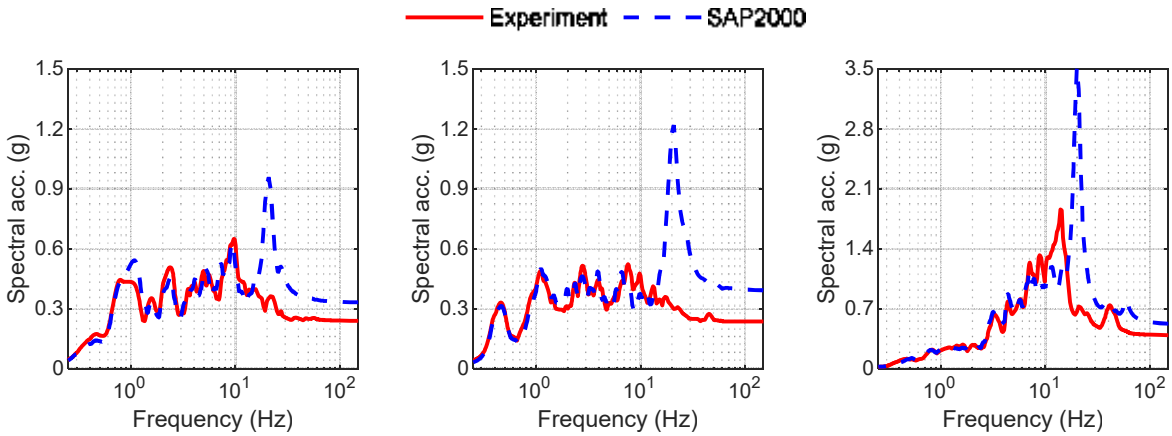

a) *x* direction b) *y* direction c) *z* direction

Figure 7. Acceleration response spectra directly above the isolation plane, test SF1B-3D

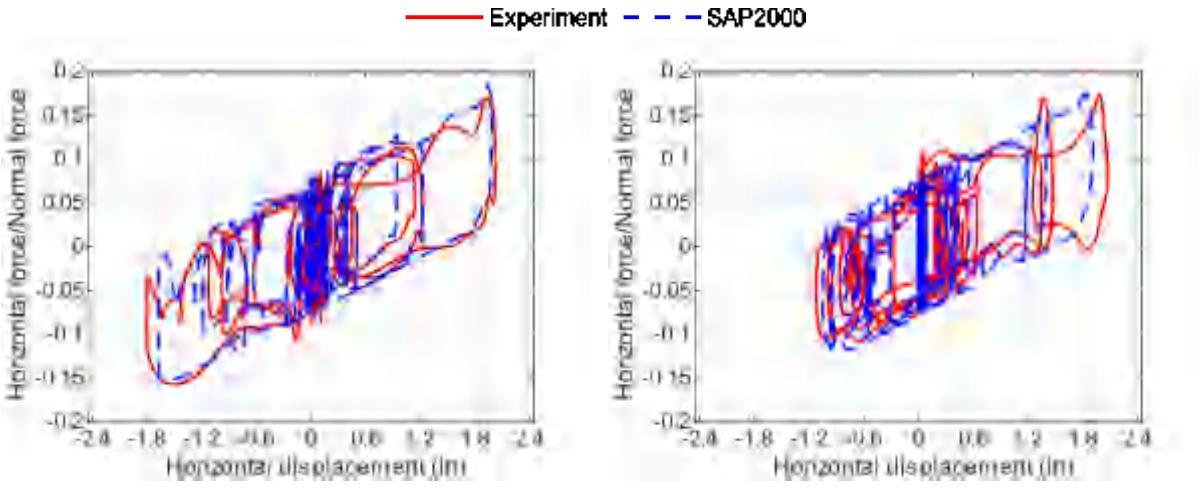

a) *x* direction b) *y* direction

Figure 8. Normalized force-displacement loops for the isolation system, test SF1B-3D

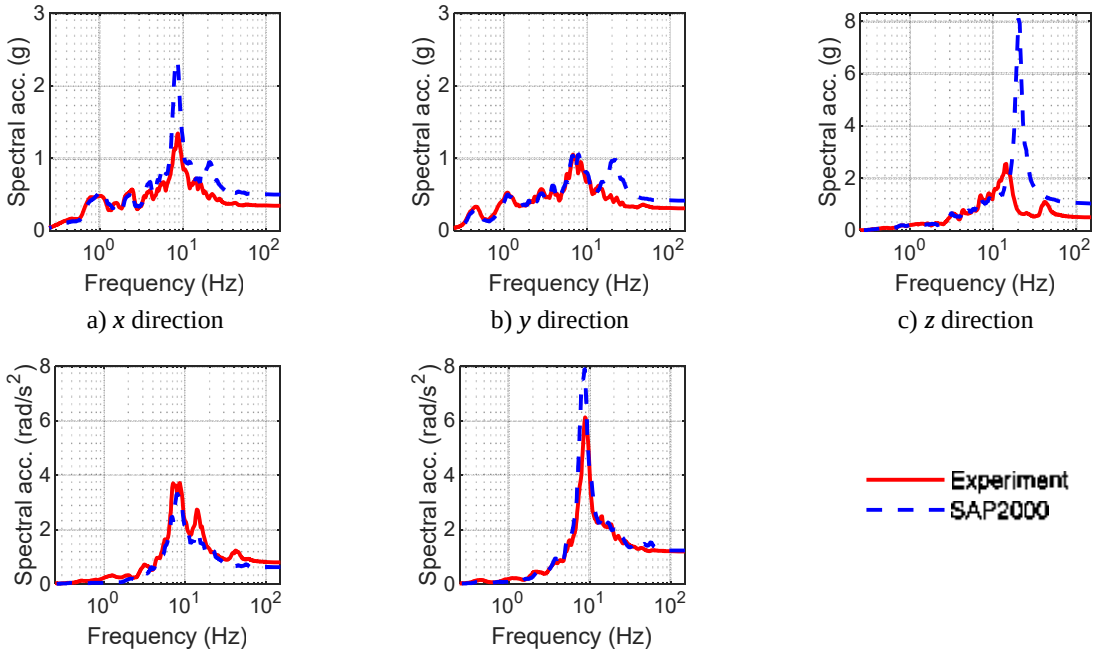

a) *x* direction b) *y* direction c) *z* direction

d) rocking about *x* axis e) rocking about *y* axis

Figure 9. Acceleration response spectra at the top of the vessel, test SF1B-3D

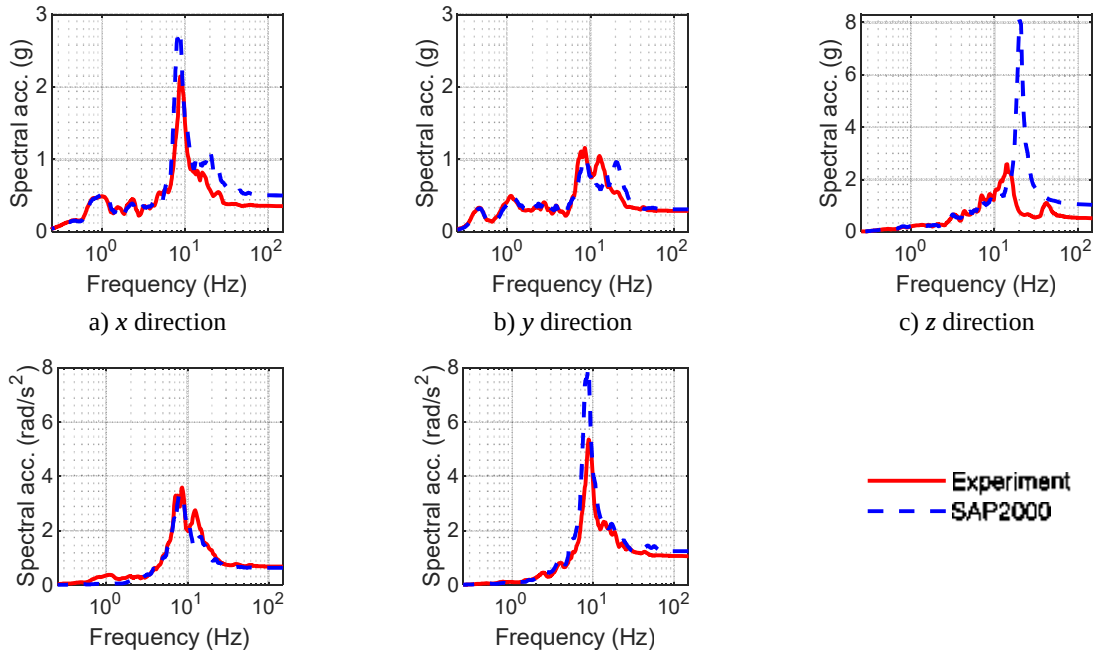

a) *x* direction b) *y* direction c) *z* direction

d) rocking about *x* axis e) rocking about *y* axis

Figure 10. Acceleration response spectra at the bottom of the vessel, test SF1B-3D

Table 4 presents the peak accelerations at the locations identified in Section 2.4.1 and the absolute percentage difference between the numerical response and the test data. The maximum isolation-system displacements and normalized forces are presented in Table 5. The predicted horizontal and rocking acceleration responses of the vessel are in good agreement with the experiment data. Differences in the vertical accelerations are attributed to the higher vertical mode frequency of the SAP2000 model: see Section 2.2. The percentage differences in the peak horizontal accelerations directly above and below the isolation plane, and at the top and the bottom of the vessel is nearly identical to that in the non-isolated configuration: 15% on average (range: 0% to 65%). The difference in the peak vertical accelerations is 32% on average (range: 0% to 106%).

The global response of the SFP isolation system is examined using normalized force-displacement loops, maximum horizontal displacements, and peak normalized forces, defined as the ratio of the horizontal force in the isolation system to the normal force on it. The agreement between the predicted and recorded normalized force-displacement loops, maximum horizontal displacements, and peak normalized forces is excellent for the larger amplitude motions, producing larger isolation-system displacements: see Figure 8 and Table 5. The agreement was poorer for the low amplitude motions, resulting in small isolation-system displacements.

2.4.4. TFP-isolated configuration

Figures 11 through 14 present the responses of the numerical analysis of TFP-isolated model and the corresponding experimental results for test TF1B-3D, with those for other tests presented in Lal ***et al.*** (2023b). The peak accelerations at the locations identified previously and the absolute percentage difference between the predicted and experimental values are presented in Table 6. Companion results for maximum isolation-system displacements and normalized forces are presented in Table 7.

The agreement between the numerically predicted and experimentally recorded accelerations for the horizontal and rocking responses of the vessel is good. The agreement in the vertical direction is poorer with differences due to the higher vertical frequency of the SAP2000 model (see Section 2.2). The average difference in the peak horizontal (vertical) accelerations directly above and below the isolation, and at the top and bottom of the vessel is 21% (40%), with a range of 0% (0%) to 70% (129%). In some cases, analysis of the SAP2000 model over predicted the amplitude of spectral acceleration at the rocking frequency (e.g., Figures 13a, 13e, 14a, and 14e) because the damping ratios in the rocking modes were not calibrated for specific seismic inputs: see Section 2.3.

Identical to the SFP-isolated configuration, the predicted normalized force-displacement loops (maximum isolation-system displacements and peak normalized forces) of the TFP isolation system are in excellent agreement with the test data for the larger amplitude motions: see Figure 12 (Table 7).

2.4.5. Discussion

The results in Section 2.4.2, 2.4.3, and 2.4.4 above demonstrate that the behavior of a mid-height isolated vessel and its isolation system is predictable. The acceleration response of the vessel in the two horizontal directions is in good agreement with the test data. The rocking response of the vessel is also captured well by the numerical models. The larger differences in the vertical acceleration response are due to the differences in the predicted and measured vertical mode frequencies. The predicted normalized force-displacement loops of the isolation systems are in excellent agreement with the experimental data.

The error thresholds for benchmarking of a numerical model are problem- and response-specific. Ipek ***et al.*** (2021) presents a validation exercise for a seismically isolated six-story building model tested on an earthquake simulator using unidirectional inputs. Differences of 35% and 65% of the recorded response were reported for the numerically predicted peak isolator displacements and floor accelerations, respectively. Given the complexity of the test specimen herein and the use of 3D seismic inputs (and the rocking of the earthquake-simulator platform), the numerical models are considered benchmarked and are utilized next to investigate the utility and quantify the benefits of mid-height seismic isolation.

Table 4. Peak accelerations[1] (g) for the 3D tests in the SFP-isolated configuration

Test		Below isolation plane			Above isolation plane			Vessel bottom			Vessel top		
		x	***y***	***z***	***x***	***y***	***z***	***x***	***y***	***z***	***x***	***y***	***z***
SF1A-3D	Experiment	0.30	0.30	0.16	0.13	0.12	0.21	0.22	0.22	0.34	0.22	0.24	0.34
	SAP2000	0.42	0.47	0.13	0.11	0.11	0.19	0.21	0.21	0.39	0.23	0.2	0.38
	Diff (%)	40	57	19	15	8	10	5	5	15	5	17	12
SF1B-3D	Experiment	0.82	0.77	0.30	0.24	0.23	0.39	0.36	0.29	0.52	0.34	0.31	0.50
	SAP2000	0.76	0.80	0.37	0.33	0.38	0.51	0.50	0.30	1.02	0.50	0.42	1.03
	Diff (%)	7	4	23	38	65	31	39	3	96	47	35	106
SF2A-3D	Experiment	0.24	0.26	0.20	0.11	0.11	0.21	0.20	0.14	0.32	0.19	0.19	0.32
	SAP2000	0.25	0.39	0.21	0.11	0.11	0.29	0.21	0.14	0.62	0.23	0.16	0.62
	Diff (%)	4	50	5	0	0	38	5	0	94	21	16	94
SF2B-3D	Experiment	0.69	0.48	0.38	0.24	0.18	0.57	0.39	0.27	0.83	0.36	0.27	0.83
	SAP2000	0.68	0.66	0.40	0.20	0.19	0.57	0.37	0.27	1.15	0.42	0.29	1.15
	Diff (%)	1	38	5	17	6	0	5	0	39	17	7	39
SF3A-3D	Experiment	0.16	0.25	0.05	0.10	0.11	0.06	0.11	0.20	0.07	0.14	0.22	0.07
	SAP2000	0.17	0.37	0.05	0.09	0.11	0.06	0.12	0.18	0.08	0.14	0.18	0.08
	Diff (%)	6	48	0	10	0	0	9	10	14	0	18	14
SF3B-3D	Experiment	0.19	0.46	0.10	0.13	0.17	0.11	0.14	0.21	0.13	0.17	0.23	0.13
	SAP2000	0.18	0.42	0.13	0.12	0.19	0.14	0.14	0.20	0.17	0.19	0.23	0.18
	Diff (%)	5	9	30	8	12	27	0	5	31	12	0	38

1. Peak acceleration taken spectral acceleration at 100 Hz.

Table 5. Peak isolator displacements and normalized forces for the 3D tests of the SFP-isolated configuration

		Displacement (in)		Normalized force	
Test		***x* direction**	***y* direction**	***x* direction**	***y* direction**
	Experiment	0.4	0.3	0.08	0.10
SF1A-3D	SAP2000	0.5	0.3	0.09	0.09
	Diff (%)	25	0	13	10
	Experiment	1.9	2.1	0.17	0.17
SF1B-3D	SAP2000	2.0	1.9	0.18	0.17
	Diff (%)	5	10	6	0
	Experiment	0.7	0.5	0.09	0.08
SF2A-3D	SAP2000	0.6	0.5	0.10	0.09
	Diff (%)	14	0	11	13
	Experiment	2.0	1.4	0.16	0.12
SF2B-3D	SAP2000	1.9	1.5	0.16	0.13
	Diff (%)	5	7	0	8
	Experiment	0.1	0.4	0.07	0.08
SF3A-3D	SAP2000	0.1	0.6	0.08	0.10
	Diff (%)	0	50	14	25
	Experiment	0.8	2.2	0.10	0.14
SF3B-3D	SAP2000	0.8	2.3	0.10	0.17
	Diff (%)	0	5	0	21

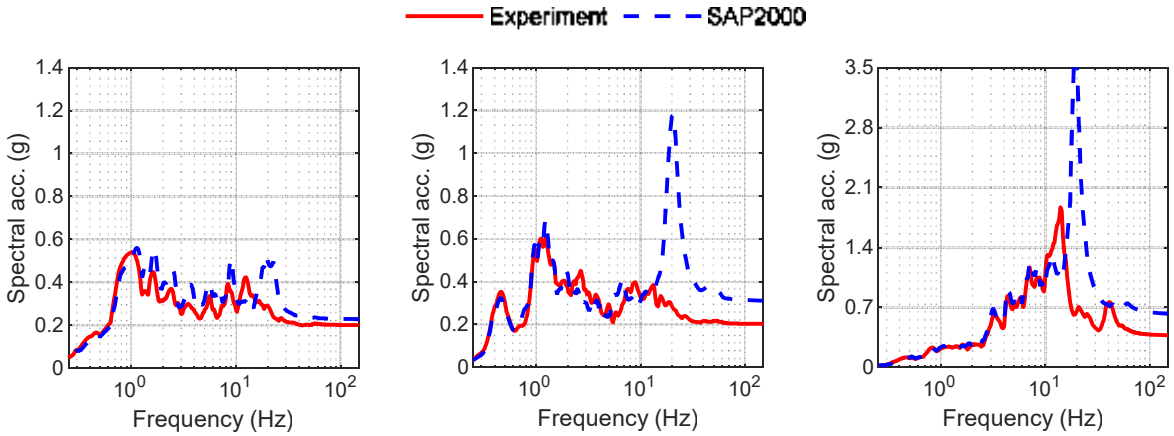

a) *x* direction b) *y* direction c) *z* direction

Figure 11. Acceleration response spectra directly above the isolation plane, test TF1B-3D

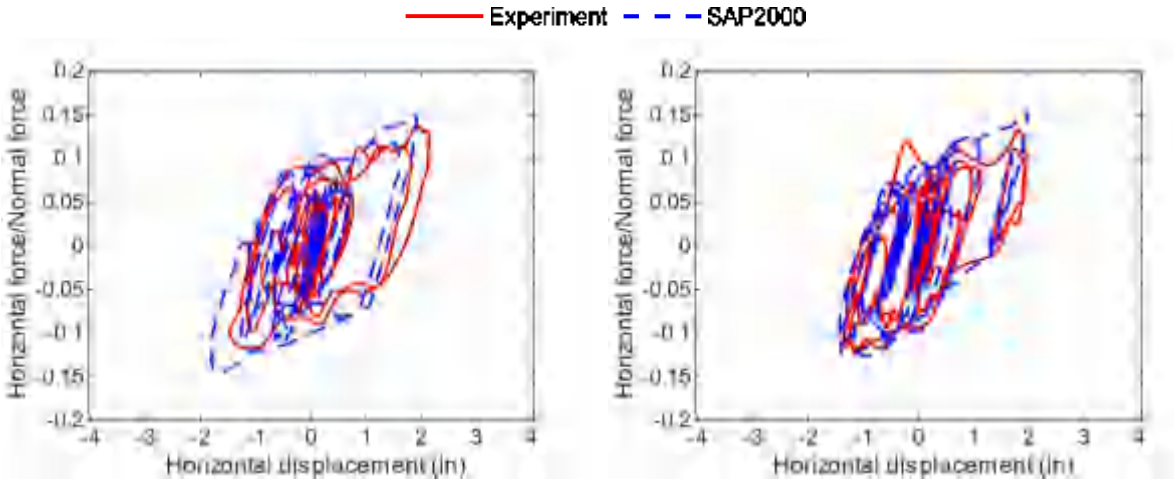

a) *x* direction b) *y* direction

Figure 12. Normalized force-displacement loops for the isolation system, test TF1B-3D

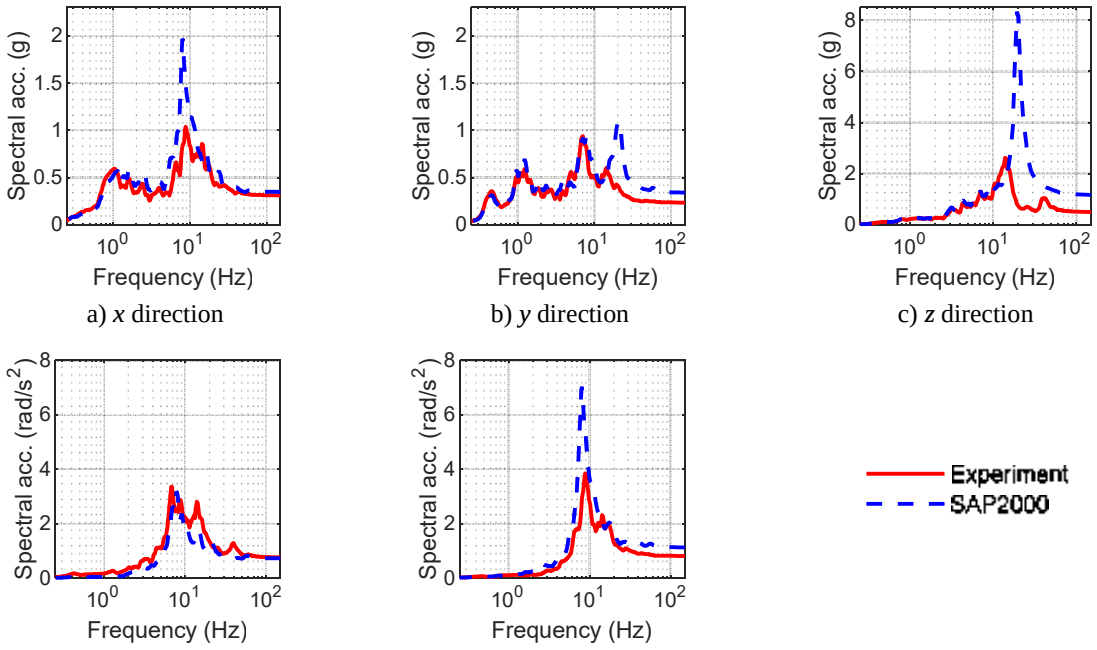

a) *x* direction b) *y* direction c) *z* direction

d) rocking about *x* axis e) rocking about *y* axis

Figure 13. Acceleration response spectra at the top of the vessel, test TF1B-3D

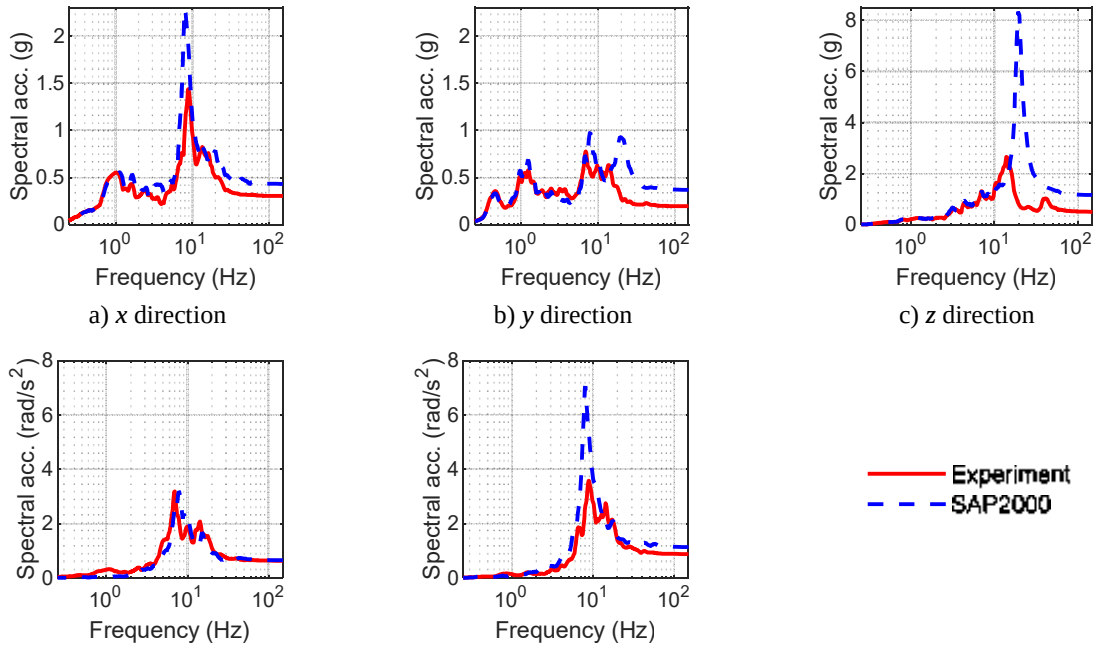

a) *x* direction b) *y* direction c) *z* direction

d) rocking about *x* axis e) rocking about *y* axis

Figure 14. Acceleration response spectra at the bottom of the vessel, test TF1B-3D

Table 6. Peak accelerations[1] (g) for the 3D tests of the TFP-isolated configuration

Test		Below isolation plane			Above isolation plane			Vessel bottom			Vessel top		
		x	***y***	***z***	***x***	***y***	***z***	***x***	***y***	***z***	***x***	***y***	***z***
	Experiment	0.30	0.27	0.12	0.10	0.11	0.15	0.13	0.13	0.19	0.13	0.17	0.19
TF1A-3D	SAP2000	0.30	0.24	0.15	0.12	0.14	0.20	0.20	0.16	0.37	0.21	0.2	0.37
	Diff (%)	0	11	25	20	27	33	54	23	95	62	18	95
	Experiment	0.81	0.85	0.31	0.20	0.20	0.37	0.30	0.20	0.50	0.31	0.23	0.49
TF1B-3D	SAP2000	0.80	0.88	0.42	0.23	0.31	0.61	0.43	0.34	1.12	0.35	0.34	1.12
	Diff (%)	1	4	35	15	55	65	43	70	124	13	48	129
	Experiment	0.32	0.32	0.21	0.17	0.12	0.28	0.24	0.15	0.43	0.18	0.14	0.42
TF2A-3D	SAP2000	0.31	0.30	0.20	0.15	0.16	0.31	0.23	0.18	0.62	0.23	0.18	0.62
	Diff (%)	3	6	5	12	33	11	4	20	44	28	29	48
	Experiment	1.07	0.87	0.58	0.29	0.22	0.70	0.48	0.31	1.20	0.33	0.3	1.21
TF2B-3D	SAP2000	0.90	0.81	0.53	0.30	0.26	1.12	0.39	0.35	1.69	0.42	0.39	1.7
	Diff (%)	16	7	9	3	18	60	19	13	41	27	30	40
	Experiment	0.11	0.18	0.05	0.07	0.11	0.05	0.07	0.14	0.06	0.09	0.15	0.06
TF3A-3D	SAP2000	0.10	0.16	0.04	0.09	0.12	0.05	0.11	0.15	0.07	0.12	0.14	0.07
	Diff (%)	9	11	20	29	9	0	57	7	17	33	7	17
	Experiment	0.24	0.56	0.14	0.14	0.18	0.17	0.13	0.21	0.18	0.14	0.2	0.18
TF3B-3D	SAP2000	0.24	0.52	0.15	0.14	0.22	0.15	0.17	0.23	0.20	0.21	0.23	0.2
	Diff (%)	0	7	7	0	22	12	31	10	11	50	15	11

1. Peak acceleration taken as spectral acceleration at 100 Hz

Table 7. Peak isolator displacements and normalized forces for the 3D tests of the TFP-isolated configuration

		Displacement (in)		Normalized force	
Test		***x* direction**	***y* direction**	***x* direction**	***y* direction**
TF1A-3D	Experiment	0.4	0.5	0.07	0.09
	SAP2000	0.5	0.6	0.10	0.10
	Diff (%)	25	20	43	11
TF1B-3D	Experiment	2.1	1.9	0.14	0.13
	SAP2000	1.9	2.0	0.15	0.15
	Diff (%)	10	5	7	15
TF2A-3D	Experiment	1.4	0.7	0.13	0.10
	SAP2000	1.3	0.9	0.12	0.12
	Diff (%)	7	29	8	20
TF2B-3D	Experiment	3.5	2.9	0.19	0.19
	SAP2000	3.0	2.9	0.18	0.18
	Diff (%)	14	0	5	5
TF3A-3D	Experiment	0.2	0.8	0.06	0.11
	SAP2000	0.3	1.1	0.09	0.12
	Diff (%)	50	38	50	9
TF3B-3D	Experiment	1.0	3.1	0.11	0.17
	SAP2000	1.1	3.1	0.13	0.18
	Diff (%)	10	0	18	6

3. Utility and benefits of mid-height seismic isolation

3.1.1. Overview

In this section, the benchmarked numerical models of Section 2 are utilized to perform response-history analyses to investigate the utility of mid-height seismic isolation and to quantify its benefits. Various stiffnesses of the vessel support frame, isolation-system properties, and ground motions were considered to answer the following three questions:

1. Is mid-height seismic isolation feasible and beneficial if the support frame of the vessel is stiff or flexible?
2. Is mid-height seismic isolation beneficial for a range of isolation-system properties?
3. Are more onerous testing requirements needed for seismic isolators used for equipment protection?

3.1.2. Support structure stiffnesses

Two support conditions were considered for the vessel by modifying the stiffness of the frame (grey in Figure 3a) in SAP2000:

1. *Near rigid*, achieved by increasing the elastic modulus of the frame material by a factor of 10, to model a piece of equipment supported near the basemat of a reactor building, wherein the ground motions are not (significantly) filtered by the building response and the seismic inputs at the points of attachment of equipment are broad banded.
2. *Flexible*, achieved by reducing elastic modulus of the frame material by a factor of 4, to model a piece of equipment supported above the basemat of a reactor building, wherein the ground motions from the basemat to the point of attachment of the equipment are amplified and filtered by the building response, and the seismic inputs (for the equipment) are narrow banded, with spectral peaks near the modal frequencies of the building. (See for example the HTGR building in Figure 4 of Parsi *et al.* (2022) where the steam generator and the reactor vessel are supported on a floor slab approximately 40 ft above the basemat.)

3.1.3. Isolation systems

Six isolation systems (IS) were utilized for the study, all consisting of SFP bearings but with different isolation periods and coefficients of friction, with the properties listed in Table 8. At the assumed model length scale of 0.5 for the cylindrical vessel herein, isolation periods of 1.06, 1.5, and 2.12 seconds were considered. At the prototype scale, these would correspond to isolation periods of 1.5, 2.12, and 3 seconds, respectively. A more flexible isolation system (with a larger isolation period) generally enables a larger reduction in accelerations, but the tradeoff is larger displacements in the bearings and on the umbilical lines crossing the isolation interface. This is discussed in more detail in Section 3.1.6. Coefficients of friction of 6% and 10% were utilized: representing values achieved with different axial pressures on the articulated slider. (See Constantinou *et al.* (2007) or Kumar *et al.* (2019) for a discussion of the relationship between coefficient of friction and axial pressure on a Friction Pendulum bearing.)

3.1.4. Seismic inputs

Two ground motions having a broad range of frequency content were utilized for the response-history analyses. Ground motions with record sequence numbers 587 (GM1) and 728 (GM2) were selected from the PEER NGA-West2 database. The time scale of all three components of the ground motions was reduced by a factor of 0.71, consistent with the assumed length scale of 0.5 for the vessel. Rotational ground motion inputs were not considered. To investigate the effectiveness of mid-height seismic isolation at different intensities of shaking, the ground motions were amplitude scaled to have geomean horizonal peak accelerations of 0.2 g, 0.4 g, and 0.6 g. Table 9 presents nomenclature for the six seismic inputs (2 ground motions, 3 intensities each).

3.1.5. Modal analyses

Analysis of the isolated and non-isolated configurations was performed to determine the modal frequencies of the vessel supported on the ***flexible*** and ***rigid*** frames. Table 10 lists the modal frequencies.

Table 8. Isolation system properties

	Sliding period[1]	Radius of curvature (R) [1,2]	Coefficient of friction		Axial stiffness[3]
			μ_{max}	μ_{min}	
IS1	1.06 seconds	11 inches	0.06	0.03	3075 kip/in^2
IS2	1.06 seconds	11 inches	0.10	0.05	
IS3	1.5 seconds	22 inches	0.06	0.03	
IS4	1.5 seconds	22 inches	0.10	0.05	
IS5	2.12 seconds	44 inches	0.06	0.03	
IS6	2.12 seconds	44 inches	0.10	0.05	

1. At the assumed model length scale of 0.5.
2. The SFP bearings and its sliders were assumed to be of the same height and diameter, respectively, as those in Lal *et al.*, (2023a; 2023b).
3. The axial stiffness was assumed to be $0.15 \times EA / L$, where E = 29,000, A = 1.77 in^2 (area of slider), and L = 2.5 (height of the bearing) based on the experimental characterization in Lal *et al.* (2023b).

Table 9. Nomenclature for the six seismic inputs

	Geomean horizontal PGA (g)	**Vertical PGA (g)**
GM1A	0.20	0.11
GM1B	0.40	0.22
GM1C	0.60	0.33
GM2A	0.20	0.24
GM2B	0.40	0.49
GM2C	0.60	0.73

Table 10. Modal analysis results for the isolated and non-isolated configurations (Hz)

	Non-isolated		**Isolated**	
	***Rigid* frame**	***Flexible* frame**	***Rigid* frame**	***Flexible* frame**
Rocking of vessel (about x and y axes)	12.4	8.3	9.5[1]	7.4[1]
Horizontal modes (x and y directions)	26	9.6	0.47/0.66/0.94[2]	0.47/0.66/0.94[2]
Vertical mode (z direction)	33	21	22.5[1]	17.5[1]

1. These values are lower than the corresponding frequencies in the non-isolated configuration due to the added vertical flexibility from the SFP bearings.
2. Corresponds to the isolated modes of the vessel with isolation periods of 2.12, 1.5, and 1.06 seconds.

3.1.6. Response-history analyses results and discussion

Response-history analyses were performed for the non-isolated and isolated configurations of the vessel using the numerical models of Section 2. A total of 84 cases were analyzed: 12 for the non-isolated configuration (2 support structures stiffnesses, 6 seismic inputs) and 72 for the isolated vessel (2 support structure stiffnesses, 6 isolation systems, 6 seismic inputs). The results extracted from the analyses include:

1. Acceleration histories at the top of the support frame on the north-east side. See location ***F1*** marked by the solid pink circle in Figure 4.
2. Acceleration histories at the top (location ***V3***) and the bottom (location ***V2***) of the vessel on the north face and at the mid-height of the vessel (location ***V1***) on the north-east side.
3. Displacement and force histories of the SFP bearings. Identical displacement and force histories were obtained for the three isolator links; the *x*- and *y*-direction histories for the north-east link were utilized.

3.1.6.1 Acceleration response at the top and the bottom of the vessel

Acceleration response spectra at the top and the bottom of the vessel were analyzed to answer the first question of Section 3.1.1. Figures 15 and 16 present the acceleration response spectra at the top of the non-isolated and IS3 isolated vessel, respectively, for GM1B. Acceleration response spectra for other isolation systems and seismic inputs are presented in Lal *et al.* (2023b). In the non-isolated configuration, the horizontal response of the vessel at its top is significantly greater when supported on the *flexible* frame: compare the red and green dashed lines in panels a and b of Figure 15. The seismic inputs were significantly amplified by the support frame (from location ***B*** to ***F1*** in Figure 4) when it is *flexible*, with further amplification by the vessel (from location ***F1*** to ***V2***/***V3***). Amplification of the seismic inputs by the *rigid* support frame (from location ***B*** to ***F1***) was negligible and is due primarily to the vessel (from location ***F1*** to ***V2***/***V3***). The horizontal responses of the isolated vessel supported on the *flexible* and *rigid* frames are virtually identical: compare the red and green dashed lines in panels a and b of Figure 16. Similar results were obtained for the other isolation systems and seismic inputs: see Lal *et al.* (2023b) for details. This outcome is expected because the flexibility afforded by the isolators is more than an order of magnitude greater than that of the support frames.

Mid-height seismic isolation is effective at reducing horizontal spectral accelerations in equipment with respect to their non-isolated counterpart for a range of support structure stiffnesses. Importantly, horizontal spectral accelerations enabled by mid-height seismic isolation are not significantly affected by the support structure stiffness. The seismic qualification of equipment is a significant contributor to capital cost (Lal *et al.*, 2022). The response reductions afforded by mid-height isolation will simplify the qualification calculations for the vessel and its internals, assuming qualification is based primarily on analysis. Importantly, the seismic spectral demands in the isolated configuration are by-and-large independent of support configuration, meaning that the vessel could be seismically qualified once but for multiple support structure stiffnesses.

The rocking-induced responses in the *x*- and *y*-directions at approximately 10 Hz in the non-isolated vessel (see Figures 15a and 15b) are effectively eliminated in the isolated vessel (see Figures 16a and 16b). The vertical response of the vessel was a function of the frequency content of the input motion and the modal frequencies of the vessel-frame system in the *z* direction. The peaks in spectral accelerations for the non-isolated (isolated) vessel represent the vertical modes at frequencies of 21 Hz (17.5 Hz) and 33 Hz (22.5 Hz) for the *flexible* and *rigid* frames, respectively, as identified in Table 10. Peak vertical accelerations in the non-isolated and the isolated vessels are reported in Lal *et al.* (2023b). Although peak vertical accelerations greater than 1 g were predicted in the vessel for GM1C, GM2B, and GM2C, which led to zero instantaneous axial load on the bearings, isolation was effective in reducing its horizontal acceleration response.

To answer the second question of Section 3.1.1 and to quantify the benefits of mid-height isolation for the vessel studied herein, ratios of peak geomean horizontal accelerations at the top of the non-isolated vessel to those in the isolated vessel, termed as an acceleration reduction factor (ARF), are presented in Tables 11 (*rigid* frame) and 12 (*flexible* frame). The corresponding maximum isolation-system displacements are also reported. Mid-height seismic isolation can reduce horizontal spectral accelerations in equipment across a range of isolation-system properties and seismic inputs. The peak accelerations at the top of the isolated vessel are smaller by a factor of between 1.5 and 6 (5 and 20) with respect to those on the non-isolated vessel supported on the *rigid* (*flexible*) frame. The maximum isolation-system displacements are between 0.2 inch and 6.6 inches.

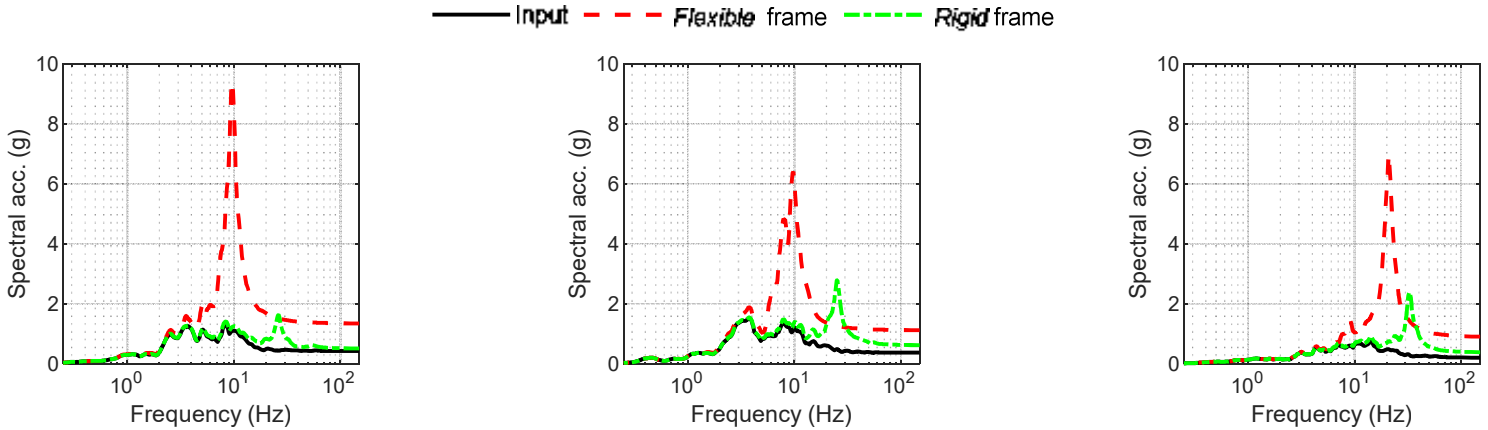

a) *x* direction b) *y* direction c) *z* direction

Figure 15. Acceleration response spectra at the top of the vessel, non-isolated, GM1B, 5% damping

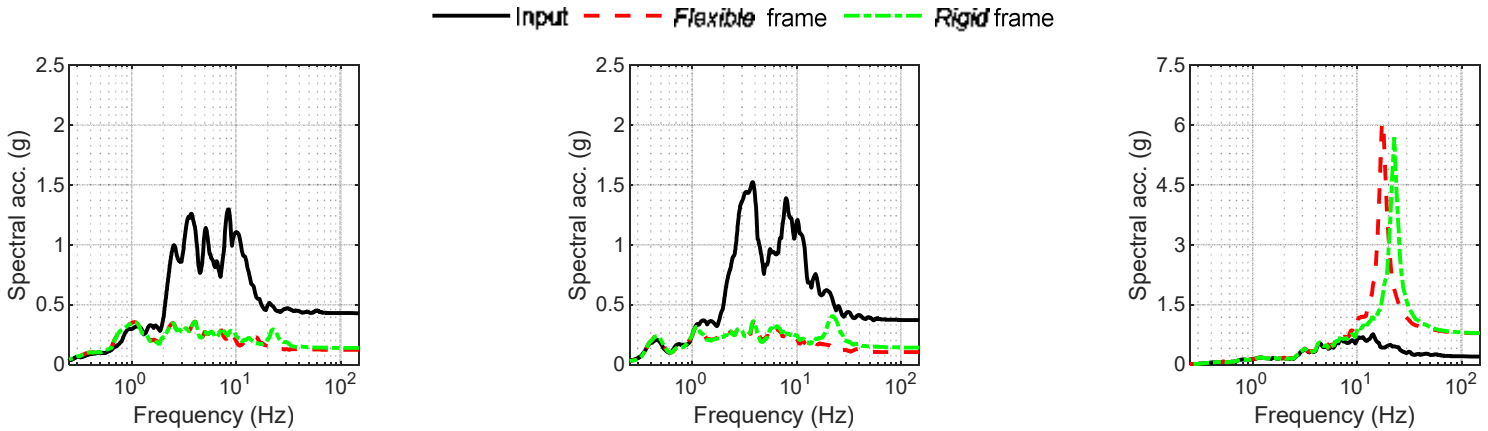

a) *x* direction b) *y* direction c) *z* direction

Figure 16. Acceleration response spectra at the top of the vessel, IS3 isolated, GM1B, 5% damping

Table 11. Acceleration reduction factors[1] (ARF) and maximum isolation-system displacements (inches) for the vessel supported on the *rigid* frame

		GM1A	GM1B	GM1C	GM2A	GM2B	GM2C
IS1 isolated (1.06 sec, 6%)	ARF	2.8	2.7	[2]	1.7		
	Maximum isolation-system displacement	0.5	1.4		2.0		
IS2 isolated (1.06 sec, 10%)	ARF	2.2	2.6	2.4	2.1		
	Maximum isolation-system displacement	0.2	1.0	1.9	0.6		
IS3 isolated (1.5 sec, 6%)	ARF	3.3	4.1	3.6	2.9	2.6	
	Maximum isolation-system displacement	0.5	1.4	2.9	1.3	4.2	
IS4 isolated (1.5 sec, 10%)	ARF	2.3	3.3	3.3	2.4	2.3	
	Maximum isolation-system displacement	0.2	1.1	2.1	0.8	2.8	
IS5 isolated (2.12 sec, 6%)	ARF	3.8	5.2	5.5	3.4	3.8	
	Maximum isolation-system displacement	0.5	1.7	3.1	1.5	4.6	
IS6 isolated (2.12 sec, 10%)	ARF	2.3	3.5	3.9	2.5	2.9	2.9
	Maximum isolation-system displacement	0.3	1.3	2.4	1.0	3.5	6.6

1. Ratio of peak geomean horizontal acceleration at the top of the non-isolated vessel to that in the isolated vessel.
2. Results are not reported for the cells highlighted in red because the maximum isolation-system displacements exceed the *soft* limit of 0.2*R*; see Section 5.4.6.2 and Appendix C of Lal *et al.* (2023b).

Table 12. Acceleration reduction factors[1] (ARF) and maximum isolation-system displacements (inches) for the vessel supported on the *flexible* frame

		GM1A	GM1B	GM1C	GM2A	GM2B	GM2C
IS1 isolated (1.06 sec, 6%)	ARF	9.3	9.9	[2]	5.2		
	Maximum isolation-system displacement	0.5	1.4		1.7		
IS2 isolated (1.06 sec, 10%)	ARF	7.4	9.8	10.0	6.4		
	Maximum isolation-system displacement	0.3	1.0	2.0	0.7		
IS3 isolated (1.5 sec, 6%)	ARF	11.8	14.8	14.0	9.3	6.5	
	Maximum isolation-system displacement	0.5	1.5	2.9	1.3	4.2	
IS4 isolated (1.5 sec, 10%)	ARF	7.4	12.6	13.6	6.9	6.7	
	Maximum isolation-system displacement	0.3	1.1	2.1	0.9	2.8	
IS5 isolated (2.12 sec, 6%)	ARF	12.7	18.6	19.7	10.6	11.6	
	Maximum isolation-system displacement	0.6	1.7	3.2	1.6	4.6	
IS6 isolated (2.12 sec, 10%)	ARF	7.4	13.1	16.1	7.3	8.3	7.8
	Maximum isolation-system displacement	0.3	1.3	2.4	1.0	3.5	6.6

1. Ratio of peak geomean horizontal acceleration at the top of the non-isolated vessel to that in the isolated vessel.
2. Results are not reported for the cells highlighted in red because the maximum isolation-system displacements exceed the ***soft*** limit of 0.2***R***; see Section 5.4.6.2 and Appendix C of Lal ***et al.*** (2023b).

For the same coefficient of friction, the ARF is generally greater for the more flexible isolation system, but the tradeoff is larger displacements in the bearings and across the isolation interface. For example, compare the ARFs and maximum isolation-system displacements for IS2 (1.06 sec, 10%) and IS6 (2.12 sec, 10%) for seismic input GM1C in Table 11: the ARF increased from 2.4 to 3.9 as the maximum isolator displacement increased from 1.9 inches to 2.4 inches. Although a smaller peak horizontal acceleration is beneficial for equipment design, safety-related umbilicals crossing the isolation plane will have to be designed and qualified to accommodate larger displacements.

3.1.6.2 Energy demands on isolators

Consensus standards ASCE/SEI 4-16 (ASCE, 2017) and ASCE/SEI 43-19 (ASCE, 2021) present requirements for prototype and production testing of seismic isolators. Five fully reversed cycles of loading to user-specified displacements for design-basis and beyond-design-basis shaking are the key seismic tests, where five is based on normalized dissipated energy calculations presented in Warn and Whittaker (2007) for base-isolated structures.

To examine if five fully reversed cycles is also sufficient for testing isolators used for equipment protection, calculations were performed for the six isolation systems of Section 3.1.3, the six ground motions of Section 3.1.4, and the two support structures of Section 3.1.2 (i.e., ***rigid*** frame and ***flexible*** frame). Results are presented in Table 13 as normalized energy dissipated (NED) per Warn and Whittaker (2007), namely, the ratio of the total energy dissipated by an isolator during one ground motion to the energy dissipated in one fully reversed cycle of loading to the maximum displacement computed for that ground motion. Values of NED are presented for the north-east isolator, noting that the values for the west and south-east isolators were essentially identical. The range for NED is between 2.1 and 5.1, confirming that five fully reversed cycles of loading is sufficient for testing isolators used to protect both structures and equipment: answering the third question of Section 3.1.1.

Table 13. Normalized energy dissipated in the north-east isolator

		GM1A	GM1B	GM1C	GM2A	GM2B	GM2C
IS1	***Rigid*** frame	2.9	3.6	[1]	3.6		
	Flexible frame	2.9	3.6		3.6		
IS2	***Rigid*** frame	3.1	3.1	3.5	3.9		
	Flexible frame	3.1	3.1	3.5	4.1		
IS3	***Rigid*** frame	2.6	3.3	3.5	4.1	5.1	
	Flexible frame	2.7	3.3	3.6	4.2	5.1	
IS4	***Rigid*** frame	2.9	2.6	3.1	2.9	4.4	
	Flexible frame	2.9	2.7	3.3	3.0	4.5	
IS5	***Rigid*** frame	2.3	2.6	3.5	3.1	4.6	
	Flexible frame	2.3	2.7	3.5	3.2	4.6	
IS6	***Rigid*** frame	2.8	2.1	2.5	2.6	3.2	4.0
	Flexible frame	2.8	2.2	2.5	2.3	3.3	4.1

1. Results are not reported for the cells highlighted in red because the maximum isolation-system displacements exceed the ***soft*** limit of 0.2***R***; see Section 5.4.6.2 and Appendix C of Lal ***et al.*** (2023b).

4. Recommendations for equipment isolation inside a nuclear facility

Consensus standards ASCE/SEI 4-16 and ASCE/SEI 43-19 provide criteria for seismic analysis and design of structures, systems, and components (SSCs) in seismically isolated, safety-related nuclear facilities, including nuclear power plants. Equipment isolation is not addressed in either ASCE/SEI 4-16 or ASCE 43-19 but will be in their next revisions. Based on the results and conclusions in this paper, three recommendations are provided for analysis and design of isolated equipment:

1. Per practice for building-level isolation, provide a horizontally stiff diaphragm above and below the isolation plane to ensure that forces and displacements in the isolators are virtually identical and predicted well by numerical analysis.
2. The axial flexibility of individual bearings must be explicitly characterized and modeled to capture the rocking and vertical responses of isolated equipment.
3. Five fully reversed cycles of loading to a user-calculated maximum displacement impose sufficient earthquake-induced energy demand on isolators for prototype and production testing of isolators, as currently proposed in ASCE/SEI 43-19 for building isolation.

Friction Pendulum bearings transmit vertical accelerations without reduction. If mitigation of vertical acceleration is important, vertical isolation and damping can be introduced.

5. Summary and conclusions

Seismic isolation is a proven technology to mitigate the effects of earthquake shaking and could enable a rapid transition to standardization of advanced reactors. Isolation of individual pieces of safety-class equipment is an alternate pathway where base isolation of reactor buildings is either impractical or cost prohibitive. To implement equipment isolation, advanced reactor developers will rely on seismic analysis tools that can accurately predict the response of isolated equipment and its isolation system and will need guidelines for their design. Herein, numerical models were developed for a mid-height supported tall, slender vessel that could represent an advanced reactor, a steam generator, or a heat exchanger. The twin goals of modeling were to 1) investigate the utility and quantify the benefits of mid-height seismic isolation, and 2) provide analysis and design recommendations for equipment isolation in a nuclear facility.

Models were developed for the non-isolated and isolated configurations of the vessel and benchmarked using the earthquake-simulator test data of Lal *et al.*, (2023a; 2023b). Shell and beam elements were used to model the vessel and its support frame. Link elements were utilized to model the Friction Pendulum bearings. Predicted acceleration response at the top, bottom, and mid-height of the vessel, and the normalized force-displacements loops for the isolation systems were compared with the test data. Good agreement was obtained between the predicted and recorded horizontal and rocking responses of the vessel. Differences in the vertical response were due in large part to the significant differences between the measured and predicted frequencies in the *z* direction. The predicted normalized force-displacement loops for the SFP and TFP isolation systems were also in good agreement with the test data. Comparison of predicted and recorded responses demonstrate that the global response of a mid-height isolated tall, slender vessel and its isolation system can be predicted accurately using currently available structural analysis software such as SAP2000. If the vessel is filled with fluid, as was the case herein, the fluid response can be treated as impulsive, and the weight of fluid can be distributed uniformly to the walls of the vessel along its height, for the purpose of predicting the global response of the vessel and its isolation system.

The benchmarked numerical models were used to perform 84 response-history analyses to investigate the utility and quantify the benefits of mid-height seismic isolation for different frame stiffnesses (***near rigid*** or ***flexible***) supporting the vessel, isolation system properties, and seismic inputs. Six SFP isolation systems were considered, with isolation periods of 1.06, 1.5, and 2.12 seconds and coefficients of friction of 6% and 10%. Two ground motion triplets, each with three intensities of shaking were utilized for analyses.

The results demonstrated that mid-height seismic isolation of a tall, slender equipment is feasible and beneficial for a range of support structures stiffnesses, seismic inputs, and isolation-system properties, with very significant reductions in the horizontal accelerations possible with respect to those in non-isolated equipment. The peak horizontal accelerations at the top of the isolated vessel were reduced by a factor of between 1.5 and 20 from those on the non-

isolated vessel. The greatest reductions in horizontal accelerations were achieved using the more flexible isolation system but the tradeoff was larger displacements in the bearings. (Any safety-related umbilical line crossing the isolation plane would have to be designed and qualified for a fraction of the displacements in the isolation system, as determined by its assigned Seismic Design Category.) Importantly, reductions in horizontal spectral accelerations enabled by mid-height seismic isolation are by-and-large independent of support structure stiffness: the reductions were similar for the vessel supported on a ***rigid*** and a ***flexible*** frame. Accordingly, an isolated piece of equipment could be seismically qualified once, but for multiple support conditions. Requirements for seismic testing of isolators used for equipment protection were investigated by calculating the normalized energy dissipated by SFP bearings for different isolation systems, seismic inputs, and support conditions. Recommendations for analysis and design of isolated equipment inside a nuclear facility are provided.

Although the focus herein was on safety-class equipment in advanced nuclear power plants, the results are applicable to tall, slender equipment regardless of industry sector. The outcomes are not specific to the spherical sliding bearings used in the experiments but are broadly applicable to mid-height, seismically isolated equipment.

Acknowledgements

The information, data, or work presented herein was funded by the Advanced Research Projects Agency-Energy (ARPA-E), U.S. Department of Energy, under Award Number DE-AR0000978. The views and opinions of the authors expressed herein do not necessarily state or reflect those of the U.S. Government or any agency thereof. The authors thank Dr. Michael C. Constantinou at the University at Buffalo for his input on numerical analysis of isolated structures.

6. References

Aiken, I. D., Clark, P. W., and Kelly, J. M. (2002). "Experimental testing of reduced-scale seismic isolation bearings for the advanced liquid metal reactor." ***Proceedings: IAEA-TECDOC-1288, Verification of analysis methods for predicting the behaviour of seismically isolated nuclear structures***, International Atomic Energy Agency (IAEA), Vienna, Austria.

American Society of Civil Engineers (ASCE). (2017). "Seismic analysis of safety-related nuclear structures and commentary." ***ASCE/SEI 4-16***, Reston VA.

American Society of Civil Engineers (ASCE). (2021). "Seismic design criteria for structures, systems, and components in nuclear facilities." ***ASCE/SEI 43-19***, Reston VA.

Constantinou, M. C., Whittaker, A. S., Kalpakidis, Y., Fenz, D. M., and Warn, G. P. (2007). "Performance of seismic isolation hardware under service and seismic loading." ***Technical Report MCEER-07-0012***, University at Buffalo, State University of New York, Buffalo, NY.

Computers and Structures Incorporated (CSI). (2021). Computer Program SAP2000 (Version 23.3.0), Berkeley, CA.

Ersoy, S., Ala Saadeghvaziri, M., Liu, G.-Y., and Mau, S. T. (2001). "Analytical and experimental seismic studies of transformers isolated with friction pendulum system and design aspects." ***Earthquake Spectra***, 17(4), 569-595.

Huang, Y.-N., Whittaker, A. S., and Luco, N. (2008). "Performance assessment of conventional and base-isolated nuclear power plants for earthquake and blast loadings." ***Technical Report MCEER-08-0019***, University at Buffalo, State University of New York, Buffalo, NY.

Huang, Y.-N., Whittaker, A. S., Kennedy, R. P., and Mayes, R. L. (2009). "Assessment of base-isolated nuclear structures for design and beyond-design basis earthquake shaking." ***Technical Report MCEER-09-0008***, University at Buffalo, State University of New York, Buffalo, NY.

Ipek, C., Wolff, E. D., and Constantinou, M. C. (2021). "Accuracy of analytical models to predict primary and secondary system response in seismically isolated buildings." *Soil Dynamics and Earthquake Engineering*, 150, 106944.

Kong, D. (2010). "Evaluation and protection of high voltage electrical equipment against severe shock and vibrations." *PhD dissertation*, University at Buffalo, State University of New York, Buffalo, NY.

Kumar, M., Whittaker, A. S., and Constantinou, M. C. (2017a). "Extreme earthquake response of nuclear power plants isolated using sliding bearings." *Nuclear Engineering and Design*, 316, 9-25.

Kumar, M., Whittaker, A. S., Kennedy, R. P., Johnson, J. J., and Kammerer, A. (2017b). "Seismic probabilistic risk assessment for seismically isolated safety-related nuclear facilities." *Nuclear Engineering and Design*, 313, 386-400.

Kumar, M., Whittaker, A. S., and Constantinou, M. C. (2019). "Seismic isolation of nuclear power plants using sliding bearings." *NUREG/CR-7254*, United States Nuclear Regulatory Commision, Washington, D.C. (ML19158A513).

Lal, K. M., Parsi, S. S., Kosbab, B. D., Ingersoll, E. D., Charkas, H., and Whittaker, A. S. (2022). "Towards standardized nuclear reactors: Seismic isolation and the cost impact of the earthquake load case." *Nuclear Engineering and Design*, 386, (https://doi.org/10.1016/j.nucengdes.2021.111487).

Lal, K. M., Whittaker, A. S., and Constantinou, M. C. (2023a). "Mid-height seismic isolation of equipment in nuclear power plants." *Earthquake Engineering & Structural Dynamics*, (https://doi.org/10.1002/eqe.3798).

Lal, K. M., Whittaker, A. S., and Constantinou, M. C. (2023b). "Mid-height seismic isolation of tall, slender equipment in advanced nuclear power plants." *Technical Report MCEER-23-0001*, University at Buffalo, State University of New York, Buffalo, NY.

Lee, D., and Constantinou, M. C. (2017). "Development and validation of a combined horizontal-vertical seismic isolation system for high-voltage power transformers." *Technical Report MCEER-17-0007*, University at Buffalo, State University of New York, Buffalo, NY.

Lee, D., and Constantinou, M. C. (2018). "Combined horizontal–vertical seismic isolation system for high-voltage–power transformers: development, testing and validation." *Bulletin of Earthquake Engineering*, 16(9), 4273-4296.

Mir, F. U. H., Lal, K. M., Kosbab, B. D., Nguyen, N., Song, B., Clavelli, M., Tilow, K., and Whittaker, A. S. (2022a). "Earthquake-simulator experiments of a model of a seismically-isolated, fluoride-salt cooled high-temperature reactor." *Technical Report MCEER-22-0004*, University at Buffalo, State University of New York, Buffalo, NY.

Mir, F. U. H., Yu, C.-C., Whittaker, A. S., and Constantinou, M. C. (2022b). "Physical and numerical simulations of seismic fluid-structure interaction in advanced nuclear reactors." *Technical Report MCEER-22-0002*, University at Buffalo, State University of New York, Buffalo, NY.

Murota, N., Feng, M. Q., and Liu, G.-Y. (2005). "Experimental and analytical studies of base isolation systems for seismic protection of power transformers." *Technical Report MCEER-05-0008*, University at Buffalo, State University of New York, Buffalo, NY.

Oikonomou, K., Constantinou, M. C., Reinhorn, A. M., and Kemper Jr, L. (2016). "Seismic isolation of high voltage electrical power transformers." *Technical Report MCEER-16-0006*, University at Buffalo, State University of New York, Buffalo, NY.

Parsi, S. S., Lal, K. M., Kosbab, B. D., Ingersoll, E. D., Shirvan, K., and Whittaker, A. S. (2022). "Seismic isolation: A pathway to standardized advanced nuclear reactors." *Nuclear Engineering and Design*, 387, (https://doi.org/10.1016/j.nucengdes.2021.111445).

Sarlis, A. A., and Constantinou, M. C. (2010). "Modelling Triple Friction Pendulum isolators in program SAP2000." *Internal report*, University at Buffalo.

Tajirian, F. F. (1992). "Seismic analysis for the ALMR." *Proceedings: International Atomic Energy Agency (IAES) Specialists' Meeting on Seismic Isolation Technology*, San Jose, CA.

Warn, G. P., and Whittaker, A. S. (2007). "Performance estimates for seismically isolated bridges." *Technical Report MCEER-07-0024*, University at Buffalo, State University of New York, Buffalo, NY.

Yu, C.-C., Bolisetti, C., Coleman, J. L., Kosbab, B., and Whittaker, A. S. (2018). "Using seismic isolation to reduce risk and capital cost of safety-related nuclear structures." *Nuclear Engineering and Design*, 326, 268-284.

Yu, C. C., and Whittaker, A. S. (2020). "Analytical and numerical studies of seismic fluid-structure interaction in liquid-filled vessels." *Technical Report MCEER 20-0003*, University at Buffalo, State University of New York, Buffalo, NY.